



Viscous and impact demagnetization of Martian crust

Hosein Shahnas^{1,2} and Jafar Arkani-Hamed^{1,2}

Received 25 February 2005; revised 20 July 2006; accepted 6 November 2006; published 23 February 2007.

[1] Magnetization of Martian crust has been modified by impact-induced shock waves and viscous decay since the cessation of the core dynamo of Mars at around 4 Gyr ago. Thermal evolution models of Mars suggest that the potentially magnetic layer was about 85 km thick during the active period of the core dynamo, assuming magnetite as the major magnetic carrier. The lower boundary of the magnetic layer has gradually decreased, by a total of about 30 km, through viscous decay of magnetization. The large impacts that created the giant basins Hellas, Argyre, and Isidis have almost completely demagnetized the crust beneath the basins. The shock wave pressure produced by impacts that created craters of diameters 300–1000 km is expected to significantly demagnetize the crust beneath the craters. However, except for a few craters, there is no signature of appreciable demagnetization. This implies that either the magnetic carriers have high coercivity and have resisted demagnetization, or magnetic source bodies are deep seated, or they have acquired magnetization after the intensive impact cratering period. An alternate possibility is that the scaling laws proposed for small craters do not apply to the large craters considered in this paper.

Citation: Shahnas, H., and J. Arkani-Hamed (2007), Viscous and impact demagnetization of Martian crust, *J. Geophys. Res.*, 112, E02009, doi:10.1029/2005JE002424.

1. Introduction

[2] The lack of a core field at present indicates that the strong magnetic anomalies of Mars detected by Mars Global Surveyor [Acuna *et al.*, 1999] arise from remanent magnetization of the crust that was acquired during the active period of the core dynamo, likely prior to 4 Gyr ago [e.g., Connerney *et al.*, 1999; Arkani-Hamed, 2004]. The absence of magnetic signature associated with giant impact basins Hellas, Isidis and Argyre indicates that the core dynamo was inactive or weakly active, for at least 100 Myr following the impacts that created these basins [Mohit and Arkani-Hamed, 2004]. The magnetization acquired by the lower parts of the crust in the presence of the magnetic field of the upper crust, as they cooled below the magnetic blocking temperatures of their magnetic carriers, after the cessation of the core dynamo is found to be small [Arkani-Hamed, 2003, 2005].

[3] During the active period of the core dynamo, bottom of the potentially magnetic layer was defined by the Curie isotherms of major magnetic carriers of the crust. The upper part of the layer was subjected to many demagnetizing factors, such as impact-induced shock waves, impact heating, volcanism, and near surface hydration. The large impacts that have created the giant basins on Mars have

completely demagnetized the crust [Acuna *et al.*, 1999]. Quantitative studies of impact demagnetization indicate that the giant impacts have almost completely demagnetized the crust within a distance of ~ 0.8 of the basin radius, and partially demagnetized the crust to distances of ~ 1.4 of the basin radius [Mohit and Arkani-Hamed, 2004]. More extensive demagnetization has also been suggested [Hood *et al.*, 2003; Kletetschka *et al.*, 2004]. If the major part of the crustal magnetization was acquired prior to the intensive cratering period occurred around 4 Gyr ago, then upper parts of the crust could have been demagnetized by impacts. It is possible that deeper part of the crust that was magnetized by the core field has lost part of its magnetization by being heated above the Curie temperature of its magnetic carriers and by gradual viscous decay of magnetization at high temperatures close to the magnetic blocking temperatures of the magnetic minerals. The thickness of the potentially magnetic layer has been reduced from top and bottom since the cessation of the core dynamo.

[4] This paper investigates the demagnetization of Martian crust after the core dynamo ceased to exist. Although it is impossible to determine vertical variations of magnetization in the crust, it is possible to estimate the thickness of the potentially magnetic part of Mars at present using data other than the magnetic anomalies. We study possible demagnetization of the crust by impacts, using craters with clear topographic signatures and a range of diameters between 300 and 1000 km [Frey *et al.*, 2002; Frey, 2003]. The correlation between the craters and magnetic anomalies is used to estimate the properties of the magnetic source bodies. We also investigate the viscous decay of magnetization in the lower parts of the crust, and

¹Earth and Planetary Sciences, McGill University, Montreal, Canada.

²Now at Department of Physics, University of Toronto, Toronto, Canada.

demonstrate that the lower ~ 30 km of the crust has been partially demagnetized.

2. Impact Demagnetization of Uppermost Crust

[5] The absence of magnetic anomalies over the giant basins of Mars indicates that the crust beneath the basins is demagnetized by the impact events [e.g., *Acuna et al.*, 1999]. The reduction of magnetization by an impact can be due to three main processes. First, an impact excavates a large cavity and displaces a significant fraction of the potentially magnetic crust, spreading it over the surroundings with a random orientation. Second, the impact-induced shock wave produces high pressures and demagnetizes an appreciable part of the crust [e.g., *Halekas et al.*, 2002; *Hood et al.*, 2003; *Mohit and Arkani-Hamed*, 2004; *Kletetschka et al.*, 2004]. Third, a large fraction of the impact energy remains in the target in the form of heat [e.g., *Melosh*, 1989] and thermally demagnetizes the magnetic materials whose magnetic blocking temperatures are exceeded. If an ambient field exists, high pressures can produce shock remanent magnetization [*Cisowski and Fuller*, 1978, 1982]. Also rocks that were thermally demagnetized by impact heating acquire thermoremanent magnetization as they cool below their Curie temperatures. The re-magnetization does not occur in the absence of the core field. The ambient crustal field is not strong enough to induce significant remagnetization either [*Arkani-Hamed*, 2003, 2005]. *Kletetschka et al.* [2005] proposed a self-magnetization mechanism through which the upper crustal layer that was magnetized by the core field was capable of producing a large magnetic field and appreciably magnetizing the lower crust in the absence of the core field. The mechanism is based on extremely high mineralization, capable of producing a magnetic layer with 25–50% coarse grain hematite and having about 250–500 A/m magnetization. Although such a pervasive mineralization may occur in localized zones, it is highly unlikely that it can occur in regions with several hundred km horizontal extent and several tens of km thickness that are required to explain the strong magnetic anomalies observed over Cimmeria and Serenum Terrae. Moreover, the main conclusion of the authors is based on extrapolating millimeter scale calculations to hundreds of km scales Martian crust, which may not be adequate. For instance, a 500 km size square disk of 50 km thickness that is uniformly magnetized at 250 A/m (the thickness and magnetization are taken from the example given by the authors) produces about 25,000 to 38,000 nT magnetic field within 25 to 50 km below the disk, comparable to that quoted by the authors. But such a disk produces about 4660 nT magnetic field at the MGS mapping phase altitude of 400 km, which is greater than the observed strong magnetic anomalies by more than an order of magnitude. Indeed, the bulk (vertically integrated) magnetization of the disk is greater than that suggested by *Connerney et al.* [1999] and other investigators [*Arkani-Hamed*, 2005; *Langlais et al.*, 2004; *Whaler and Purucker*, 2005] by more an order of magnitude. A more realistic scenario reveals no appreciable magnetization of the lower crust by the magnetic field of the upper crust [*Arkani-Hamed*, 2005].

[6] Other near surface processes may also modify the magnetization of the crust. Brecciation reduces the coherent magnetization of the crust by randomizing the directions of fragmented blocks [*Scott et al.*, 1997]. Shock metamorphism and melting can result in formation of new minerals that have lower or higher susceptibility and remanent magnetism [*Pilkington and Hildebrand*, 2000; *Werner et al.*, 2002]. Melt sheets produced at terrestrial impact sites are usually highly magnetic, but they generally produce short wavelength magnetic anomalies that cannot be detectable at satellite altitudes. The short wavelength anomalies may be the consequence of local variations of the thickness of the melt sheet and/or the components of the fragments in the breccia [e.g., *Ebbing et al.*, 2001].

[7] We calculate the impact-induced shock pressure to estimate the extent of demagnetization of the crust beneath the impacts for a number of craters with diameters larger than 300 km. Thermal demagnetization due to impact heating is not considered because the spatial extent of the thermal demagnetization is likely less than that of the shock demagnetization [*Mohit and Arkani-Hamed*, 2004]. The correlation of the impact-induced demagnetized regions with the magnetic anomalies of Mars provides a means to estimate the properties of the magnetic source bodies, and age of the impacts relative to the magnetic anomalies. For a given crater diameter we determine the impact energy, the shock pressure produced, and the expected extent of demagnetization of the crust, by adopting the method by *Mohit and Arkani-Hamed* [2004] and using the Pi scaling law [*Melosh*, 1989] that relates the impactor size to the final size of the crater. Briefly, an observed crater diameter, D_o , is related to the transient diameter of the crater, D_{tr} , using the *Holsapple* [1993] scaling relationship

$$D_{tr} = 0.7576 D_o^{0.921} D_*^{0.079} \quad (1)$$

where D_* is the transition diameter from simple to complex crater, assumed 7 km for Mars [*Melosh*, 1989]. The transient diameter is then related to the kinetic energy of the projectile, E , through the *Schmidt and Housen* [1987] relationship

$$E = \{(D_{tr} U^{0.09} g^{0.22}) / 0.2212\}^{(1/0.26)} \quad (2)$$

where U is the impact velocity, and g is the gravitational acceleration at the surface of Mars. The kinetic energy is then related to the radius of the projectile for given projectile velocity and density. The majority of impact craters on Mars are created by heliocentric projectiles with 8–12 km/s velocity [*Neukum and Wise*, 1976]. We adopt an impact velocity of 10 km/s and assume a spherical projectile of basaltic composition with 2900 kg/m³ density. The radius of the isobaric core (R_o) where the peak pressure decays very slowly, here assumed constant, is set to be 0.75 of the projectile radius, and the penetration depth of the projectile is taken to be equal to the projectile radius [e.g., *Pierazzo et al.*, 1997].

[8] Using the Hugoniot equation,

$$P_o - P'_o = \rho u_s u_p \quad (3)$$

together with the empirical relationship between the particle velocity, u_p , and shock wave velocity, u_s ,

$$u_s = C + Su_p \quad (4)$$

and the power law distribution of shock pressure outside the isobaric core

$$P(r) = \rho u_o (C + Su_o (R_o/r)^n) (R_o/r)^n \quad r > R_o \quad (5a)$$

and

$$P(r) = P_o \quad r \leq R_o \quad (5b)$$

we determine the shock pressure, $P(r)$, as a function of distance r from the center of the crater, the impact site, and the pressure in the isobaric core, P_o . The un-shocked pressure P'_o is assumed to be negligible compared to the isobaric core pressure. C is the bulk sound speed ($= 3.5$ km/s) and S ($= 1.5$) is the shock parameter of the material. The values are typical for major crustal rocks [Melosh, 1989, Table AII.2]. The particle velocity in the isobaric core u_o is assumed $1/2$ of the impact velocity because the physical properties of the target and the projectile are almost identical [Melosh, 1989].

[9] Two different exponential decay models have been suggested, a constant n value of 1.87 [Melosh, 1989], and variable n values for different pressure ranges; $n = 1.2$ for $P < P_H$, and for $P > 10P_H$, and $n = 2.5$ for other pressures, where P_H ($= 5$ GPa) denotes the pressure at the Hugoniot elastic limit [Mitani, 2003]. We adopt the constant n value. Also the pressure reduction near the surface due to interference of direct and reflected waves [Melosh, 1989] is taken into consideration. The effective pressure at a point in the target is calculated by

$$P_{eff} = P - P_{ref}(1 - t/t_{rise}) \quad \text{for } t \leq t_{rise} \quad (6a)$$

and

$$P_{eff} = P \quad \text{for } t > t_{rise} \quad (6b)$$

where P is the pressure of the direct shock wave, P_{ref} is the pressure of the shock wave that is reflected at the surface, t is the difference in the arrival times of the direct and reflected waves (reflected minus direct), and t_{rise} is the risetime of shock pressure, which is approximated by the time required for a projectile to penetrate to its final depth that is equal to the radius of the projectile [Melosh, 1989]. Comparison of magnetic anomalies over areas surrounding the giant basins Hellas, Isidis, and Argyre and the calculated distribution of shock pressures shows that the crust is almost completely demagnetized at pressures $\sim 2-3$ GPa [Mohit and Arkani-Hamed, 2004]. Demagnetization pressures as low as ~ 1 GPa have also been proposed by Hood *et al.* [2003]. We assume complete demagnetizing pressure of 2 GPa throughout this paper.

[10] Figure 1 shows the shock pressure distribution induced by a projectile that creates a crater of 300 km diameter, calculated by Holsapple-Schmidt-Housen (H-S-H) and Pi scaling laws (The computer code for the Pi scaling

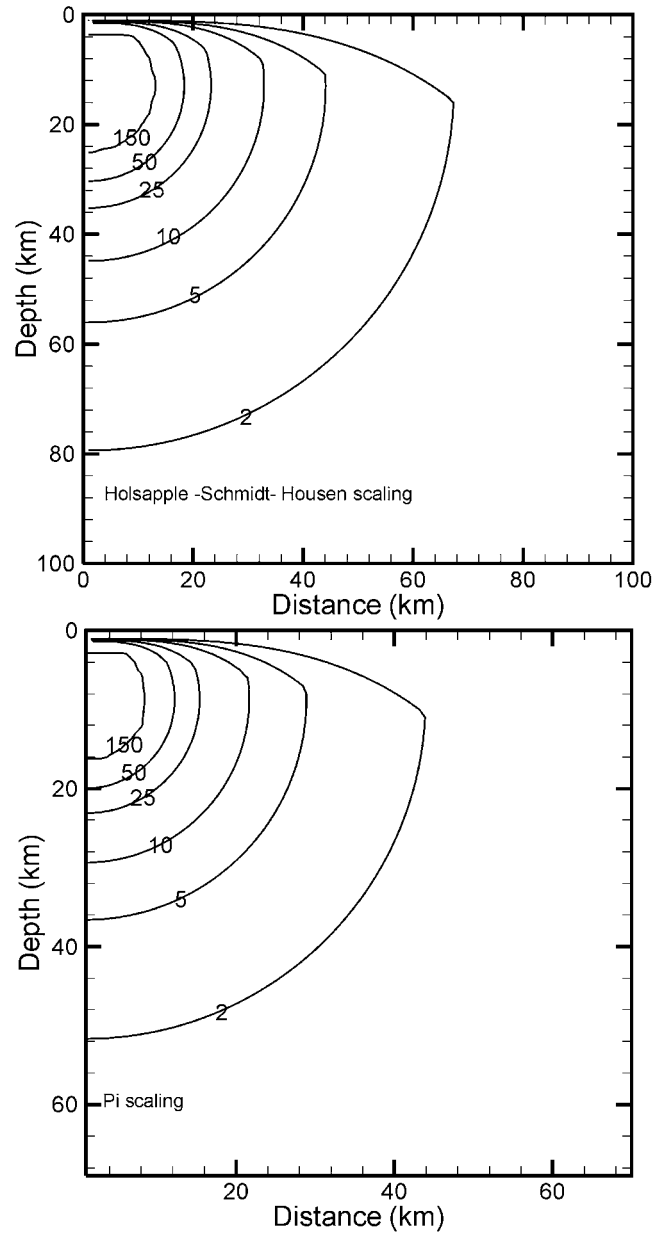


Figure 1. The shock wave pressure distribution due to an impact that creates a crater of 300 km diameter, determined using the two scaling laws. The numbers on the curves denote pressure in GPa.

was downloaded from Jay Melosh's Web site at University of Arizona, <http://www.lpl.arizona.edu/tekton/crater.html>). The sharp decrease of pressure near the surface emphasizes the interference of direct and reflected shock waves. Figure 2 displays the shock-demagnetized boundary limits determined by the two scaling laws for two impacts that create craters of 300 and 1000 km diameters. The diameters of the craters we have examined are between these two diameter values. The shock pressure inside the curves exceeds the threshold pressure of 2 GPa. Note that the curves are not concentric. The center of each curve is defined by the depth of penetration of the projectile, which is taken as the radius of the projectile [e.g., Pierazzo *et al.*,

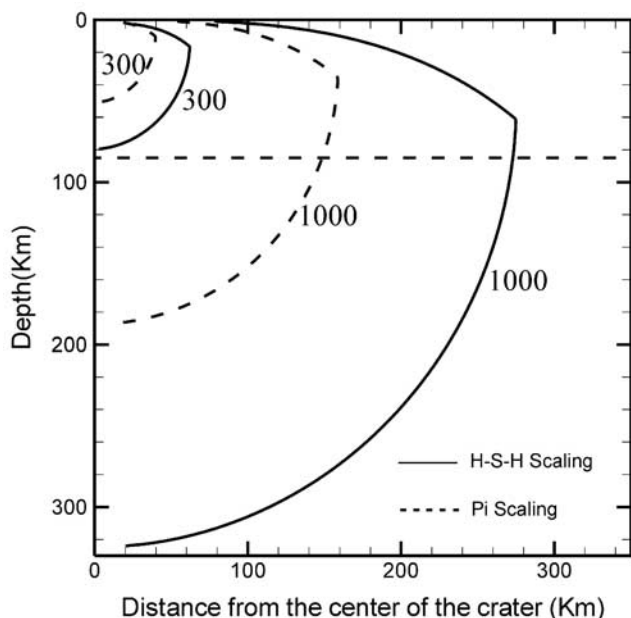


Figure 2. The demagnetization limits of the shock wave pressure due to impacts that create craters of 300 km, and 1000 km for two scaling laws. The horizontal dashed lines denote the bottom of the potentially magnetic layer, 85 km depth. The numbers on the curves are the crater diameters. The area inside a curve experiences shock pressures larger than 2 GPa, assumed to be completely demagnetized. Partial demagnetization occurs outside this area.

1997]. The demagnetized region calculated by the Pi scaling is substantially smaller than that calculated by the H-S-H scaling. This is because, for a given crater diameter the Pi scaling results in a much smaller projectile size compared to that obtained by H-S-H. The latter is almost equal to the projectile size calculated by *Gault's* [1974] empirical relationship, obtained by *Melosh's* computer code. We consider these two laws the two end-members.

[11] According to H-S-H formulation, an impact creating a crater of 300 km diameter can demagnetize a 50 km thick magnetic layer, to a horizontal distance of ~ 60 km. The demagnetization of the entire magnetic layer is extended to a horizontal distance of ~ 280 km from the center for an impact that creates a crater of 1000 km diameter. However, according to the Pi scaling law, the former impact cannot demagnetize the entire layer and the latter impact can demagnetize the entire layer to a horizontal distance of only 150 km. The potentially magnetic layer was estimated by *Arkani-Hamed* [2005] on the basis of the thermal evolution models of Mars calculated using parameterized mantle convection overlain by a growing stagnant lithosphere and assuming that magnetite is the major magnetic carrier. The potentially magnetic layer would be thinner by a factor of ~ 1.9 if pyrrhotite is the major magnetic carrier and thicker by $\sim 20\%$ if hematite is the magnetic carrier, because of their different Curie temperatures.

[12] *Turcotte et al.* [2002] suggested that the crust beneath *Cimmeria* and *Sirenum Terrae* is about 90 km thick, and *Neumann et al.* [2004] estimated a range of 5.8–102 km for the crustal thickness variations. We have considered 85 km

potentially magnetic layer in this paper. The lower parts of a 102 km thick crust remains hotter than Curie temperature during the active period of the core dynamo.

[13] The near surface region is largely excavated and partly disturbed with random orientations, even though it is not subjected to high shock pressures as emphasized by *Melosh* [1989]. This region retains no coherent direction of its previous magnetization and thus has no appreciable contributions to the observed magnetic anomalies. The transient diameter obtained by the two scaling laws (Figure 3) is comparable to the resulting crater diameter for small craters, but the ratio of the transient diameter to the final diameter decreases rapidly as the crater size increases. We assume that the region inside the transient diameter is completely demagnetized.

[14] Figure 4 shows the depth to the threshold pressure of 2 GPa directly beneath the center of a crater calculated using the Pi and H-S-H scaling laws. The depths to the threshold pressure are similar for both scaling laws when the crater diameter is small, but the difference between them increases with the increase of the crater diameter. Large impacts like those created *Utopia*, *Chryse*, *Hellas*, *Argyre*, and *Isidis*, can demagnetize the entire magnetic layer to a distance determined by the intersection of the threshold demagnetizing pressure curve with the bottom of the layer, whereas small impacts can only demagnetize part of the layer.

[15] The giant impact basins *Hellas*, *Isidis* and *Argyre* show prominent demagnetization in almost the entire floor. However, some giant basins such as *Chryse* and especially *Utopia* are in a region with almost no magnetic anomalies in the surroundings. Either some other factors that do not obviously relate to impacts have demagnetized the surroundings, or these regions were non-magnetic to start with. Figure 5 shows the magnetic intensity map of Mars at 170 km altitude obtained using Mars Global Surveyor Electron Reflectometer (MGS/ER) data [*Mitchell et al.*, 2001], shaded by the surface topography. The black color denotes the areas with no data. The 2 GPa demagnetization boundaries for the giant basins determined on the basis of the two scaling laws are also shown. The inner circle is for Pi scaling and the outer for H-S-H. The figure indicates that H-S-H scaling describes the demagnetized regions better than Pi scaling for these giant basins.

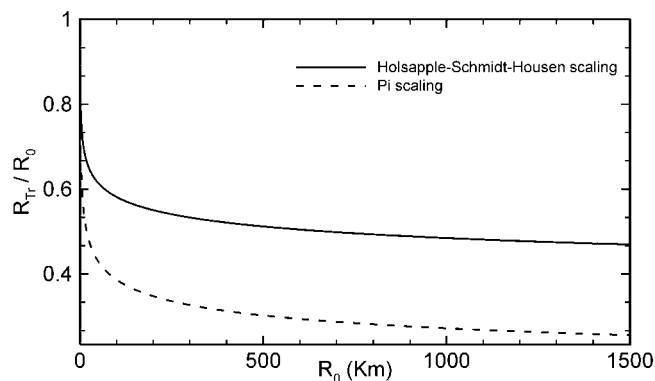


Figure 3. The ratio of transient radius, R_{tr} , to the final crater radius, R_o , as a function of R_o determined by the two scaling laws.

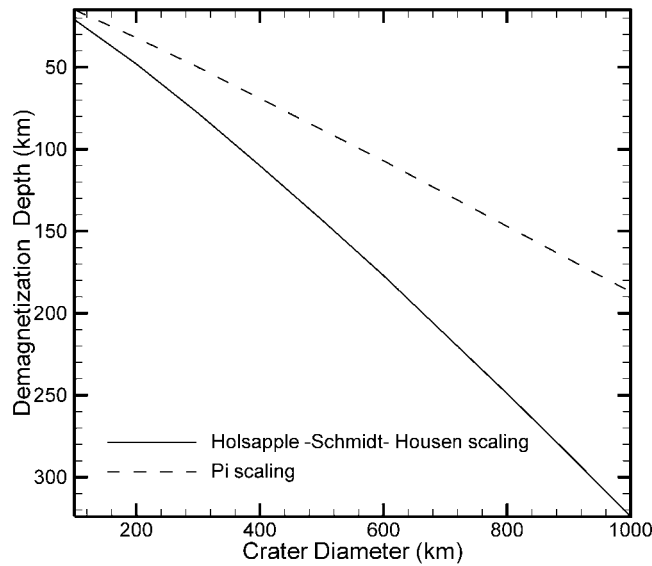


Figure 4. The completely demagnetized depth at the center of the impact crater versus the crater diameter determined using the H-S-H and Pi scaling laws.

[16] There are many visible and buried craters on strongly magnetic southern hemisphere [Frey, 2003; Frey et al., 2002] that provide an opportunity to investigate the impact demagnetization of the crust on scales smaller than those of the giant impacts. In this study we concentrate on nineteen craters with diameters larger than 300 km and with clear topographic signatures (some were downloaded from the

Mars nomenclature site, and some were provided by H. Frey (Goddard Space Flight Center, personal communication, 2005)). Table 1 lists their locations and dimensions. The three giant basins are also included in the table for comparison. For detailed study of the impact demagnetization effects, we focus on each individual crater. Two magnetic field intensity maps are used in this study. The first map is the magnetic intensity map at 170 km altitude obtained using the Electron Reflectometer data by Mitchell et al. [2001]. The second map is derived at 100 km altitude using the spherical harmonic coefficients of the 90-degree harmonic model by Cain et al. [2003]. The demagnetized regions calculated by the Pi scaling do not penetrate to the base of the layer in majority of the craters. We note that the impacts that created these craters may not have completely demagnetized the magnetic layer beneath the entire crater floors. But the interiors of the circular boundaries are expected to be fully demagnetized by the impact pressure.

[17] The probability distribution is calculated by

$$P(X \leq x) = \sum_{X' < x} P(x'), \quad X = \{x'\} \quad (7)$$

where X is the set of quantities in probability distribution calculation, x is the assumed upper limit, and $P(x')$ is the probability of finding the discrete quantity x' . We calculate the probability of demagnetization for each crater in two regions: inside a circle of radius R where the entire crust is expected to be demagnetized, and outside the circle from R to $2R$, using both scaling laws (Table 1). The minimum value of the upper limit in probability calculations is restricted by the magnetic noise. The noise contribution

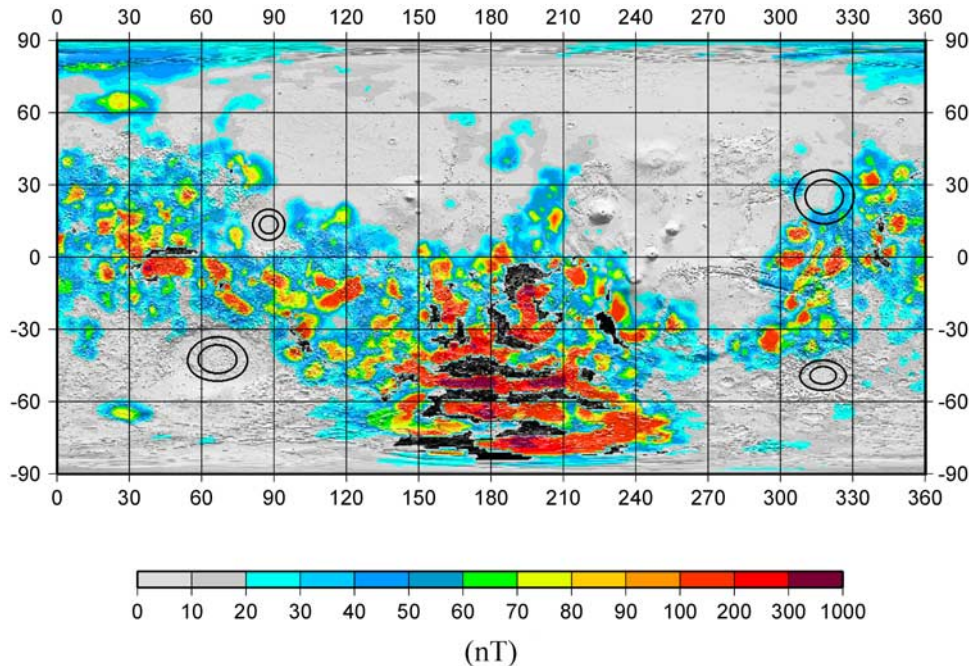


Figure 5. The magnetic intensity map at 170 km derived from the Electron Reflectometer data by Mitchell et al. [2001]. The magnetic intensity is shaded using the surface topography for better illustration of the giant impact basins. The impact-demagnetized pressure boundaries, 2 GPa, of the large basins Isidis, Chryse, Hellas, and Argyre, calculated using the H-S-H scaling (outer curves) and Pi scaling (inner curves), are superimposed over the map.

Table 1. Locations and Sizes of the Craters Investigated in This Study^a

	LAT, deg	LONG, deg	DIA, km	Magnetic Map of Ref.(a)						Magnetic Map of Ref.(b)					
				Pi Scaling			H-S-H Scaling			Pi Scaling			H-S-H Scaling		
				B _{RMS} , nT	P _{IN}	P _{OUT}	B _{RMS} , nT	P _{IN}	P _{OUT}	B _{RMS} , nT	P _{IN}	P _{OUT}	B _{RMS} , nT	P _{IN}	P _{OUT}
1* Cassini	23.6	32.0	420	50.5	0.00	0.00	50.6	0.00	0.00	80.1	0.00	0.00	85.5	0.00	0.02
2 S of Lyot	41.3	38.0	500	21.4	0.57	0.53	23.4	0.53	0.57	38.6	0.04	0.18	47.0	0.16	0.13
3 MOLA Hole	30.0	47.7	615	34.6	0.08	0.07	39.1	0.06	0.00	22.4	0.57	0.07	34.0	0.18	0.01
4* Tikhonravov	13.5	36.0	386	51.2	0.00	0.00	52.6	0.00	0.00	57.3	0.00	0.00	68.6	0.00	0.03
5* Antoniadi	21.5	61.0	410	23.6	0.00	0.00	24.0	0.19	0.14	53.2	0.00	0.00	63.9	0.00	0.00
6 Tempe Can 4	31.8	283.5	315	3.8	1.00	1.00	3.7	1.00	1.00	13.1	1.00	1.00	13.2	1.00	1.00
7 Tharsis nw tempe	53.3	284.0	600	2.7	1.00	1.00	3.0	1.00	1.00	12.0	1.00	0.98	11.4	0.98	0.87
8* Candidate A	-37.0	3.3	444	8.3	1.00	1.00	8.9	1.00	0.99	89.1	0.00	0.00	87.1	0.00	0.00
9* Schiaparelli	-2.7	16.7	471	43.8	0.00	0.00	47.1	0.00	0.06	97.1	0.00	0.00	104.6	0.00	0.00
10 Schroeter	-1.9	56.1	305	68.0	0.00	0.00	66.5	0.00	0.00	96.9	0.00	0.00	95.8	0.00	0.00
11* Huygens	-14.3	55.4	470	21.1	0.56	0.56	22.3	0.53	0.47	50.1	0.00	0.00	47.2	0.00	0.30
12 E Huygens	-13.3	63.3	380	33.4	0.00	0.00	36.4	0.00	0.00	98.0	0.00	0.00	101.1	0.00	0.00
13 Under schiaparelli	-5.9	12.3	550	22.5	0.57	0.38	27.9	0.39	0.20	108.7	0.00	0.00	109.3	0.00	0.02
14* Herschel	-14.6	129.6	315	42.5	0.00	0.00	42.7	0.00	0.00	105.1	0.00	0.00	109.3	0.00	0.00
15* de Vaucouleurs	-13.1	170.8	335	51.9	0.00	0.00	53.9	0.00	0.00	89.1	0.00	0.00	90.4	0.00	0.01
16* Newton	-40.4	201.7	308	40.7	0.00	0.00	43.6	0.00	0.00	159.3	0.00	0.00	174.8	0.00	0.00
17 Tharsis Thaumasia	-35.8	266.5	557	19.7	0.73	0.34	20.6	0.42	0.43	42.5	0.00	0.00	39.7	0.01	0.08
18 Ladon	-17.8	330.7	525	25.3	0.15	0.38	24.0	0.32	0.60	44.6	0.00	0.22	66.1	0.21	0.16
19 Holden	-25.0	327.3	610	16.7	0.82	0.57	21.5	0.62	0.49	67.6	0.10	0.02	81.1	0.03	0.08
20 Hellas	-42.3	66.4	2070	5.3	1.00	1.00	5.7	1.00	0.91	15.4	0.85	0.61	20.6	0.71	0.45
21 Isidis	13.4	87.8	1352	4.2	1.00	1.00	4.9	1.00	0.71	12.3	0.91	0.71	17.1	0.79	0.30
22 Argyre	-49.0	317.5	1315	5.0	1.00	0.98	6.9	1.00	0.85	29.1	0.52	0.77	21.2	0.70	0.46

^aLAT, LONG, and DIA stand for latitude, longitude, and diameter, respectively. B_{RMS}, P_{in}, and P_{out} are the RMS magnetic field inside the expected demagnetized region of radius R, and the probability inside demagnetization boundary and its surrounding ring, respectively. The first map, ref.(a), is the magnetic intensity map at 170 km altitude obtained using the Electron Reflectometer data by *Mitchell et al.* [2001]. The second, map ref.(b), is derived at 100 km altitude from the spherical harmonic models of the magnetic field of Mars, the 90-degree harmonic model by *Cain et al.* [2003]. The asterisk (*) denotes the craters that have also been investigated by *Mohit and Arkani-Hamed* [2004].

could be different in different places, and among different maps derived using different data and data processes. A noise of 1 nT at 400 km altitude translates to 32 or 166 nT at 100 km altitude, if the noise is characterized by spherical harmonic of degree 40 or 60, respectively. There are external field components as large as a few nT at 400 km altitude, which will give rise to appreciable noise at 100 km. An upper limit of $x = 20$ nT is considered for the noise in the probability calculations. Therefore P is the probability of an observation to be equal or less than 20 nT. Then $P = 1$ implies that all bins inside the region of interest have magnetic intensity equal or less than 20 nT. Assuming $P \geq 0.7$ as a measure of demagnetization we see that except for a few cases which show partial weakening, no clear signature of demagnetization is evident. Comparison of the probabilities inside the circles of the pressure boundaries and their surrounding rings reveals no appreciable weakening in most of these nineteen craters. Similar conclusion is obtained if the demagnetization probabilities of the giant impacts are taken as a measure of demagnetization. Figure 6 displays the diameters of the circular areas where the entire magnetic layer is expected to be demagnetized according to the two scaling laws for two different depths. An impact that creates a crater of 550 km diameter, for example, is capable of completely demagnetizing the entire magnetic layer within a circle of 88 km diameter and the upper 50 km of the layer within a circle of 150 km diameter, according to the Pi scaling law which yields lower values for the extent of demagnetization. These are roughly equivalent to the wavelengths of ~ 180 and 300 km, and are expected to be resolved in the magnetic anomaly maps adopted.

[18] The results displayed in Table 1 (ref.(a)) are for the magnetic intensity map at 170 km altitude obtained using

the Electron Reflectometer data by *Mitchell et al.* [2001]. For Pi-scaling law, crater numbers 6, 7 and 8 show demagnetization, but there is no evidence of partial weakening of the interiors compared to their surroundings. However,

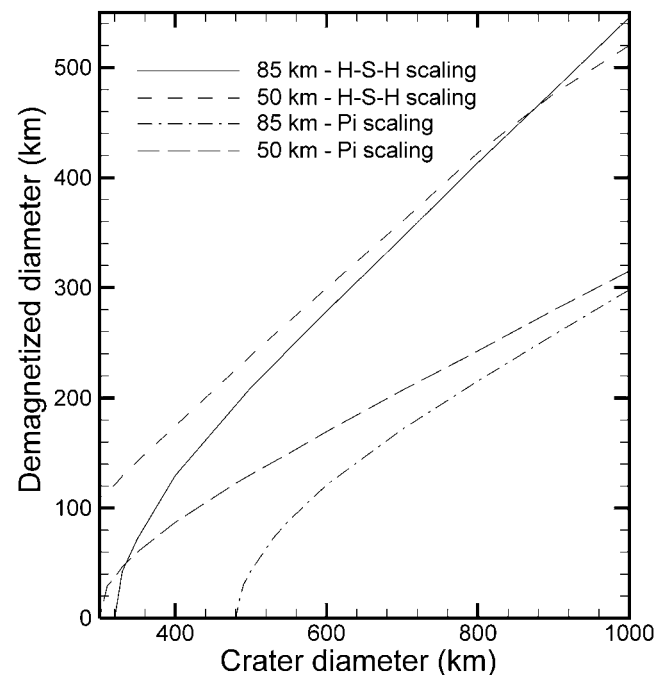


Figure 6. The expected demagnetized circular boundary diameters for 85 and 50 km depths calculated using the H-S-H and Pi scaling laws.

Table 2. Physical Parameters of the Nominal Model

Parameter	Value/Source
Radius	3390 km
Core radius	1500 km
Initial thickness of the crust	30 km
Specific heat of the mantle	1200 J/kg/K
Specific heat of the core	800 J/kg/K
Thermal expansion coefficient, mantle	3×10^{-5}
Thermal expansion coefficient, core	7×10^{-5}
Surface temperature	230 K
Elastic-ductile transition temperature	1073 K
Radioactive element content	<i>Wänke and Dreibus</i> [1994]
Radioactive content of the crust	30%
Potassium content of the core	0

magnetic weakening is observed in Tharsis Thaumasia, and Holden craters for this scaling law. The second map used in Table 1 (ref.(b)) is derived at 100 km altitude from the spherical harmonic model of *Cain et al.* [2003]. On the basis of this map, craters 6 and 7 are demagnetized. Also crater MOLA Hole show some magnetic weakening. However, the table shows no obvious correlation between the size of the crater and the weakening of the magnetic intensity. No meaningful statistical analysis can be made on the basis of only 19 craters. Only a few craters show magnetic weakening, and in a few others the magnitude of the magnetic field both in the interior and the surroundings is of the same order. There are craters for which their surroundings are less magnetized than their interiors. These observations lead us to conclude that there is no consistent evidence for appreciable impact demagnetization of the Martian crust. In the present work we have used two most recent magnetic anomaly maps. Compared to the results of *Nimmo and Gilmore* [2001] our results are consistent for the giant impacts. In our present work a higher probability represents a better crustal demagnetization and therefore based on the first map of Table 1 there is a good agreement between our results and those of *Nimmo and Gilmore* for South of Lyot. This crater, Cassini, Schiaparelli, Huygens and Under Schiaparelli of Table 1 (ref.(a)) are not demagnetized. These craters (numbers 2, 1, 9, 11, and 13 of Table 1) correspond to crater numbers 11, 16, 14, 12, and 8 of Table 1 of *Nimmo and Gilmore*. Among these impact craters there is an inconsistency only with Schiaparelli case between our results and those of *Nimmo and Gilmore*.

3. Viscous Demagnetization of Lower Crust

[19] Time evolution of depth to Curie temperature is constrained by the thermal evolution of Mars. Here we use the thermal evolution models presented by *Arkani-Hamed* [2005] that were calculated on the basis of parameterized mantle convection overlain by a thickening stagnant lithosphere and time-dependent thermal boundary layers at the top and bottom of the mantle. A total of 23 thermal evolution models were calculated in order to study effects of different physical parameters on the thermal evolution of Mars. The details of his nominal model and the major physical parameters of the other models are duplicated in Table 2 and Table 3 for easy reference. The major magnetic minerals suggested for the Martian crust [e.g., *Hargraves et*

al., 2001; *Kletetschka et al.*, 2000a, 2004; *Dunlop and Kletetschka*, 2001; *Rochette et al.*, 2001; *Dunlop and Arkani-Hamed*, 2005] are magnetite, hematite and Pyrrhotite with the Curie temperatures of 580°C, 670°C, and 320°C, respectively. The depth to Curie temperature of these minerals has been investigated by *Arkani-Hamed* [2005]. Although the depth to Curie isotherm may have increased in the last ~3.5 Gyr, the potentially magnetic layer has not thickened, because there has been no core field to magnetize the cooling lower parts. The magnetization acquired by the lower parts in the absence of the core dynamo, but in the presence of the magnetic field of the upper parts, has negligible effects on the observed magnetic anomalies [*Arkani-Hamed*, 2003, 2005].

[20] The magnetic properties of rocks are pressure dependent. However, the pressure inside the magnetic crust of Mars is not high enough to have appreciable effects on rock magnetism. The pressure increases from zero at the surface to ~0.9 GPa at the bottom of a basaltic crust of density 3000 kg/m³ and thickness 80 km. *Schult* [1970] measured the Curie temperature of synthetic titanomagnetite $\{(1-x)Fe_3O_4 - xTiFe_2O_4\}$ from zero to 6 GPa for the x values ranging from zero to 0.84. The Curie temperature increased almost linearly by about 100 degrees as pressure increased from zero to 6 GPa. Accordingly, the maximum increase of the Curie temperature in the Martian crust would be only 15C, much smaller than the uncertainty of the

Table 3. Physical Parameters of the Thermal Evolution Models^a

Model	1	2	3	4	5	6	7	8	9
1	10	E300	1700	0	16	1	10	0	0
2	10	E300	1700	0	16	1	30	0	0
3	20	E300	1700	0	16	1	20	0	0
4	20	E300	1700	0	16	1	30	0	0
5	30	E300	1600	0	16	1	30	0	0
6	30	E300	1700	0	16	0	30	0	0
7	30	E300	1700	0	16	1	10	0	0
8	30	E300	1700	0	16	1	20	0	0
9 Nominal	30	E300	1700	0	16	1	30	0	0
10	30	E300	1700	0	16	1	30	0	1
11	30	E300	1700	0	16	1	30	0	2
12	30	E300	1700	0	16	1	30	15	0
13	30	E300	1700	0	16	1	40	0	0
14	30	E300	1700	0	16	2	30	0	0
15	30	E300	1700	0	30	0	30	0	0
16	30	E300	1700	300	16	1	30	0	0
17	30	E300	1800	0	16	1	30	0	0
18	40	E300	1700	0	16	1	30	0	0
19	40	E300	1700	0	16	1	40	0	0
20	50	E300	1700	0	16	1	30	0	0
21	50	E300	1700	0	16	1	50	0	0
22	30	E540	1700	0	16	1	30	0	0
23	30	$\eta/5$	1700	0	16	1	30	0	0

^aThe columns are as follows: (1) Initial crustal thickness in km. (2) E300 denotes the activation energy of 300 KJ, E540 denotes that of 540 KJ, and $\eta/5$ means that the dynamic viscosity is 1/5 of that of the nominal model. (3) Initial temperature at the bottom of the upper thermal boundary layer in K. (4) The super heated core of 300 K extra. (5) The average Uranium content at present in ppb. (6) The radioactive model: 1, *Wänke and Dreibus* [1994]; 2, *Lodders and Fegley* [1997]; 0, *Turcotte and Schubert* [1982] terrestrial. (7) The percentage of the total radioactive elements of the planet concentrated in the crust. (8) The percentage of Potassium of the total planet concentrated in the core. (9) Thermal expansion coefficient: 0, constant (3×10^{-5}); 1, linear increase with radial distance; 2, quadratic increase with the radial distance.

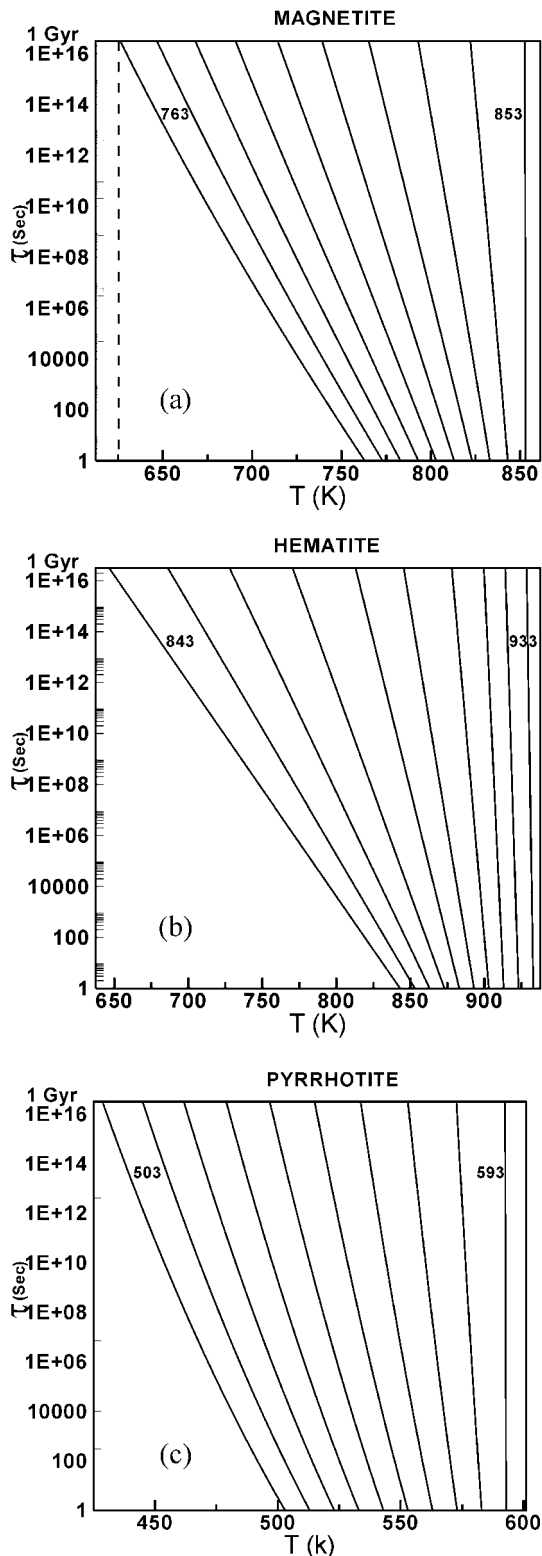


Figure 7. The relaxation time versus temperature of (a) magnetite, (b) hematite, and (c) pyrrhotite. The vertical dashed line in Figure 7a shows that the partial magnetization acquired by magnetite within blocking temperatures 750–760 K will decay in time with a relaxation time of about 1 Gyr if placed at 620K. The temperatures at $\tau = 1$ s are shown for the upper and lower temperature curves with the 10°K steps for the internal curves.

temperature distribution in the Martian crust determined on the basis of thermal evolution models during the first 600 Myr of the planet's history when the core dynamo was likely active. *Gilder et al.* [2004] reported the lab measurements of the effects of pressure on the isothermal remanent magnetization, direct field demagnetization, and alternating field demagnetization of single domain (SD) and multi domain (MD) magnetite under pressures from zero to 6 GPa. The experiment showed that the pressure has negligible effects on these magnetic properties up to about 1 GPa, but considerable effects at higher pressures.

[21] The lower boundary of the potentially magnetic layer that was established when the core dynamo ceased to exist at ~ 4 Gyr ago has changed since, partly because of the temperature increase above the Curie temperature due to high rate of heat production by radioactive elements and partly because of the gradual viscous decay of magnetization in the absence of an ambient field. The first mechanism was studied by *Arkani-Hamed* [2005] through monitoring the temperature in the lower parts of the stagnant lid and setting the bottom of the magnetic layer to the depth of Curie isotherms of major magnetic carriers. In this paper we investigate the second mechanism, the gradual demagnetizing at the bottom of the magnetic layer due to viscous decay of magnetization.

[22] Viscous demagnetization has been measured at temperatures up to 400–550°C on single-domain and small multidomain magnetite, hematite and pyrrhotite [e.g., *Dunlop and Özdemir*, 1997, and references therein]. It is demonstrated that a magnetized rock left at a high temperature and zero ambient field gradually loses its magnetization as time passes, roughly following

$$M = M_o \text{Exp}(-t/\tau) \quad (8)$$

where M_o is the initial magnetization and M is the remaining magnetization after time t . The relaxation time τ depends on temperature and the size, shape, anisotropy, and magnetic properties of the magnetic minerals. Plots of the relaxation time as a function of temperature were constructed by *Pullaiah et al.* [1975] for magnetite and hematite, and by *Dunlop et al.* [2000] for pyrrhotite. We use these plots, and the thermal evolution models of *Arkani-Hamed* [2005] to determine the viscous decay since the cessation of the core dynamo. We assume that the magnetic blocking temperatures of magnetite, hematite and pyrrhotite continuously vary from their Curie temperatures down to 100 degrees lower than their Curie temperatures. We divide this 100-degree temperature range into 100 equal intervals, one degree per interval, and use the temperature at the middle of an interval to determine the relaxation time for the blocking temperature within that interval. Although magnetic minerals usually acquire larger portion of their magnetization at higher blocking temperatures, we assume for simplicity that partial magnetization is uniformly distributed within the 100-degree blocking temperature range, which seems reasonable in the absence of direct information about the magnetic properties of the Martian crust. For magnetite and pyrrhotite we use equation (2) of *Dunlop et al.* [2000] and their laboratory measurements of the blocking temperatures and relaxation times to calculate the relaxation time at a given temperature in the magnetic layer. For hematite, we fit

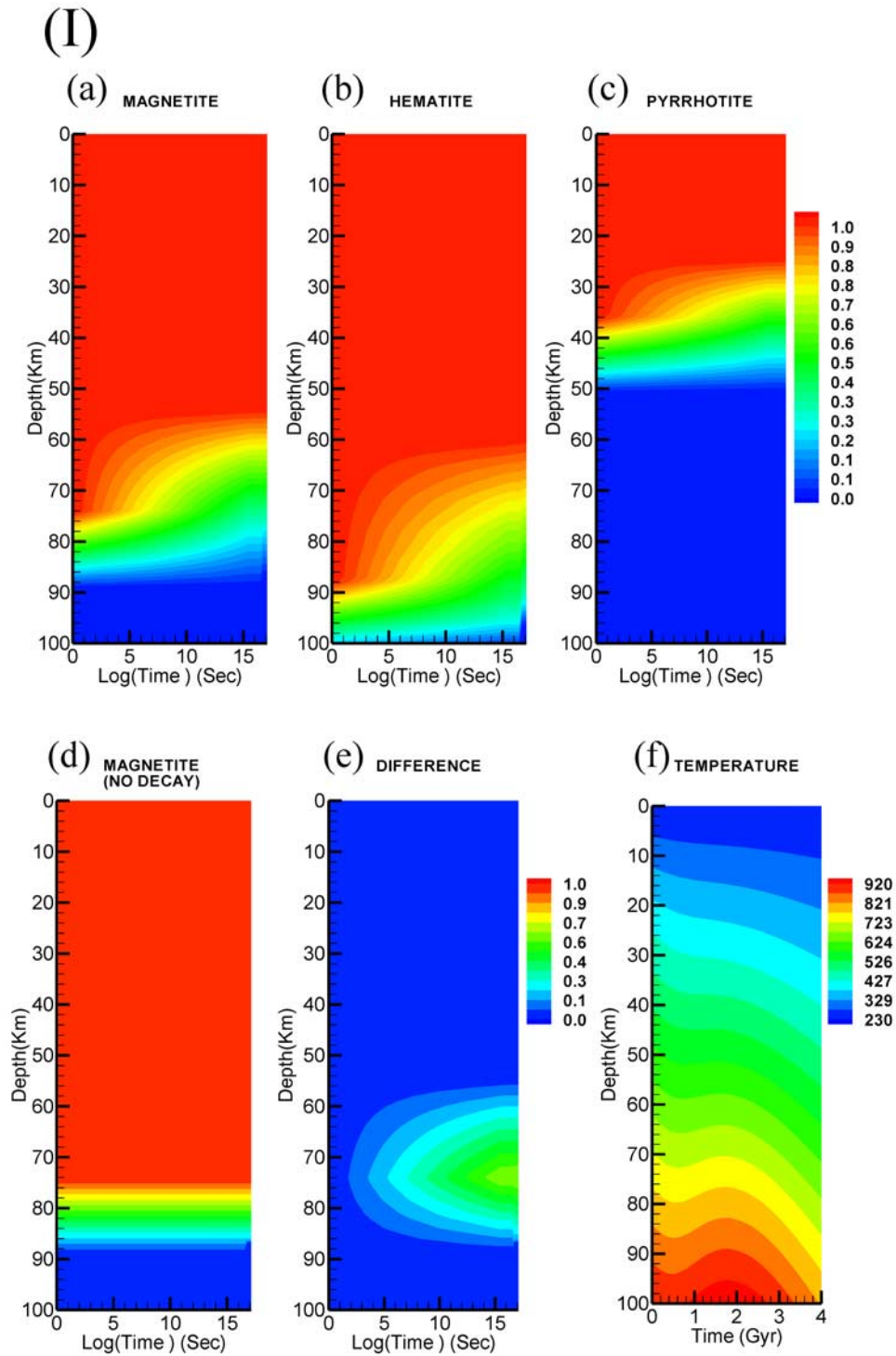


Figure 8. The normalized magnetization (normalized to 1 at 4 Gyr ago) of the magnetic layer as a function of time, for (a) magnetite, (b) hematite, and (c) pyrrhotite. (d) Thermal (with no viscous decay) and (e) viscous (only) demagnetization. (f) The thermal evolution within the upper 100 km. The I series are the nominal stagnant lithosphere model. The II and III series are for plate tectonics models operating in the first 250 Myr and 500 Myr, respectively.

lines to the $\log \tau$ versus temperature plots of *Pullaiah et al.* [1975] and interpolate the relaxation time at a given temperature using these lines. Figure 7 shows the relaxation time versus temperature curves we have adopted. Only one every 10 curves are shown for clarity purposes. As an

example, Figure 7a shows that the partial magnetization acquired within the blocking temperature range of 750–760 K by magnetite would decay in time with a relaxation time of about 1 Gyr if placed at 620K.

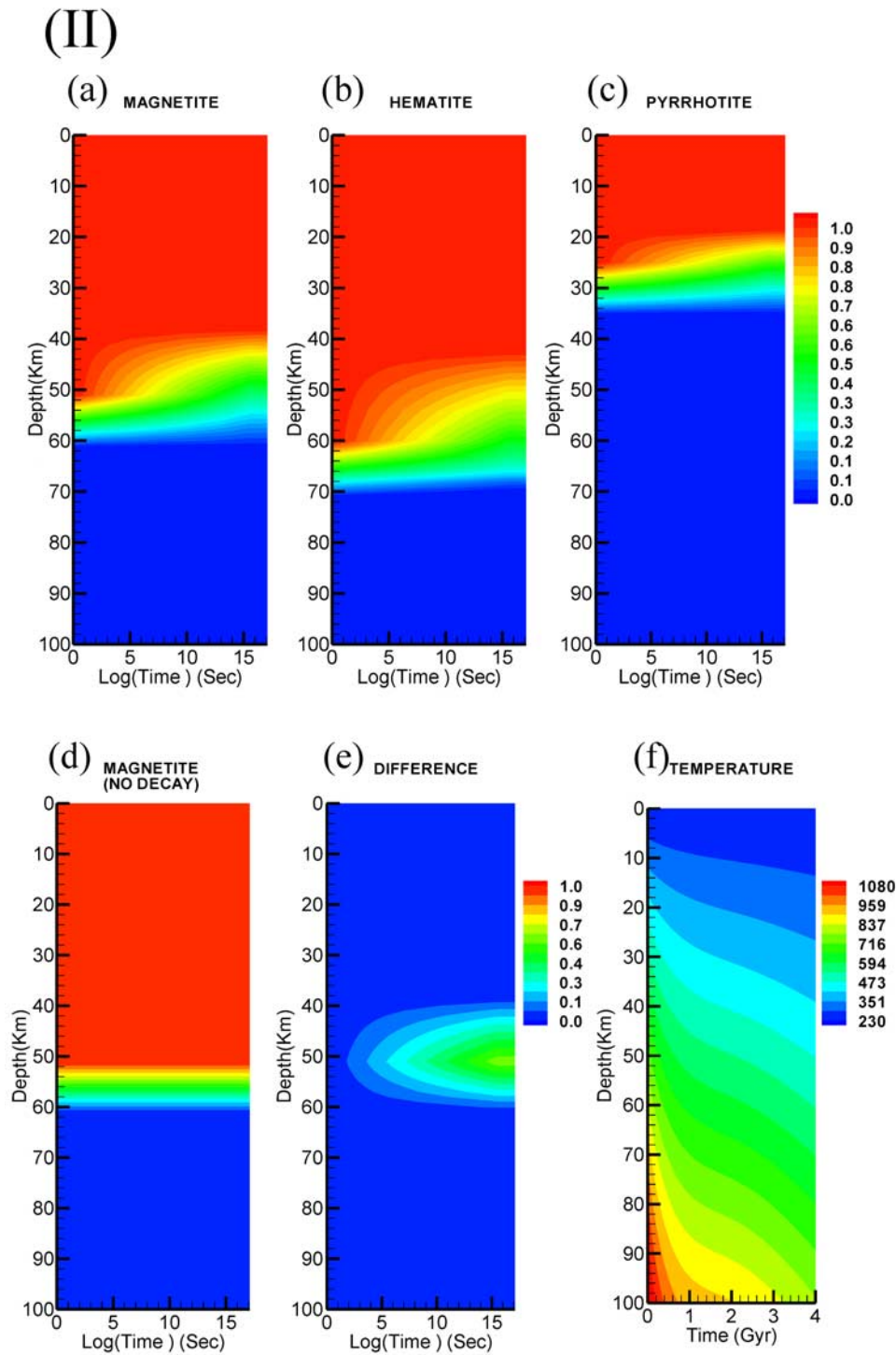


Figure 8. (continued)

[23] Figure 8 shows the demagnetization history of the potentially magnetic layer based on *Arkani-Hamed's* [2005] nominal model since the cessation of the core dynamo at 4 Gyr ago. Figures 8a, 8b, and 8c present the magnetization of the crust assuming that magnetite, hematite, or pyrrhotite are major magnetic carriers, respectively. The magnetization is normalized to the maximum value at 4 Gyr, which occurs in the regions with temperatures much lower than the blocking temperature ranges of the magnetic minerals.

The thermal evolution in the upper 100 km is displayed in Figure 8f. Because of the low temperatures, the magnetization in the upper parts of the layer has remained essentially unchanged. The temperature in the zone with the normalized magnetization between 0 and 1 immediately after the cessation of the core dynamo, for example ~ 12 km in the extreme left column of Figure 8a, is within the magnetic blocking temperature range. The zone was only partially magnetized by the core field. The lower parts of the layer

(III)

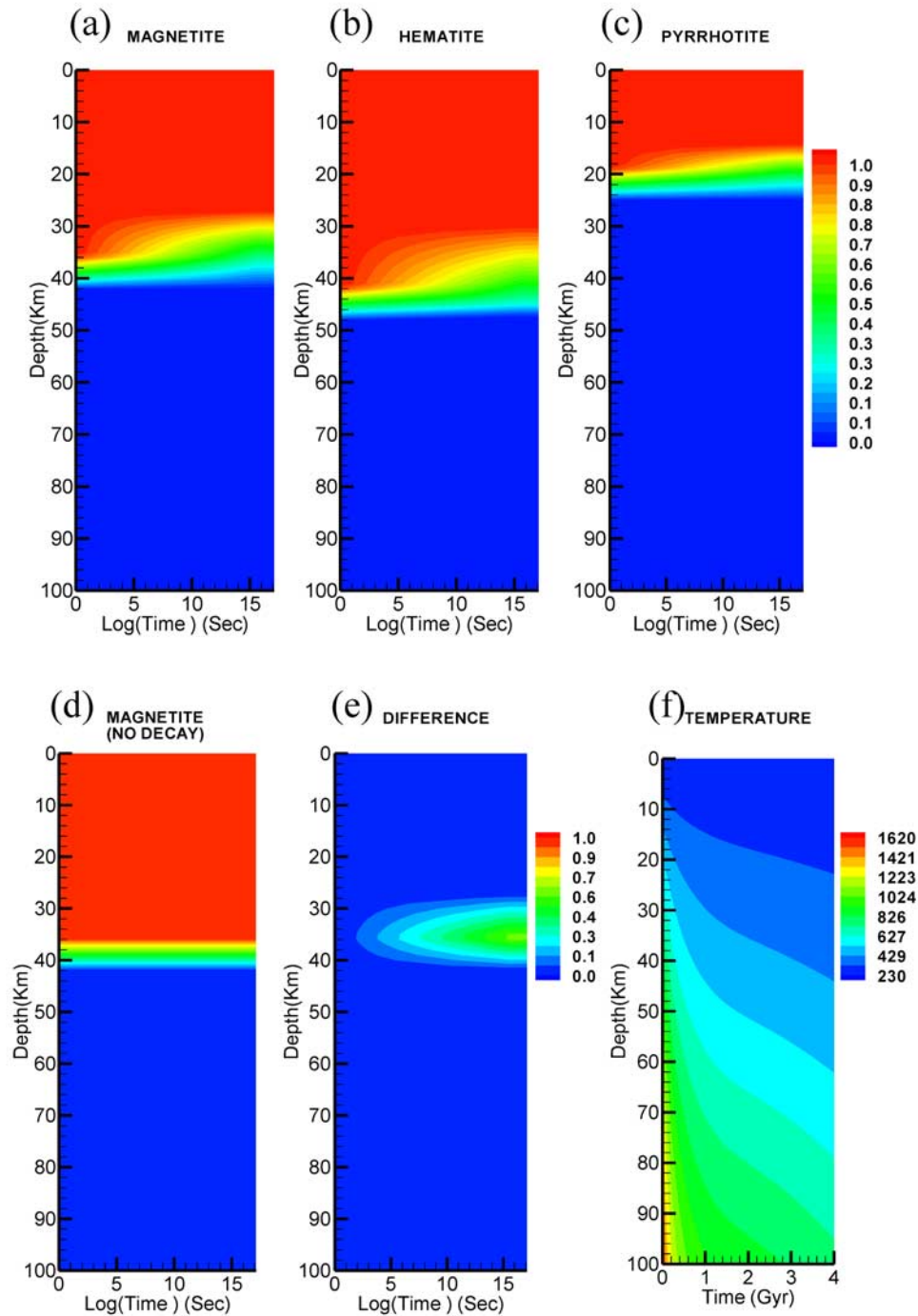


Figure 8. (continued)

lost all or part of their magnetization. The complete loss (Figure 8d) is partly due to heating of the layer above the Curie temperature after the cessation of the core dynamo and partly because of the very short viscous relaxation time at high temperatures which results in substantial decay of the magnetization. Figure 8e shows the region which has been demagnetized by viscous decay for the magnetite model. Since the cessation of the core dynamo ~ 2 km of the magnetic layer has been thermally and completely

demagnetized and another ~ 30 km has been partially demagnetized through viscous decay, if magnetite is the major magnetic carrier. The demagnetized zone is thinner for pyrrhotite because of higher thermal gradient and rapid cooling of the shallower zone, and it is thicker for hematite because of deeper magnetic zone that cools slowly allowing viscous demagnetization to have appreciable effects. The potentially magnetic layer at present must be thin (< 50 km) if pyrrhotite is the major magnetic carrier. This requires a

high concentration of pyrrhotite to give rise to observed magnetic anomalies, which seems unlikely [Dunlop and Arkani-Hamed, 2005].

[24] Whether appreciable plate tectonics were active during the early history of Mars or the planet essentially started as a one-plate planet is still debated [e.g., Sleep, 1994; Nimmo and Stevenson, 2000; Breuer and Spohn, 2003; Solomon et al., 2005]. Nimmo and Stevenson [2000] showed that the efficient cooling of the Martian mantle by early plate tectonics could allow the core to generate a strong magnetic field. The formation of the major part of the Martian crust (20–30 km) during the early chemical differentiation and gradual subsequent thickening [Norman, 1999, 2002], or gradual formation of the entire crust in the first ~ 1 Gyr [Hauck and Phillips, 2002] is not yet clear. Breuer and Spohn [2003] argued that efficient cooling of the mantle by early plate tectonics prevents formation of a ~ 50 km thick crust estimated from the surface topography and gravity of Mars. Breuer and Spohn [2006] suggest that the Martian crust was mostly produced early with gradual thickening at later times. The authors concluded that Mars became a one-plate planet at essentially very early history, and suggested a superheated core to generate a core dynamo. The thermal evolution models calculated by Arkani-Hamed [2005] showed that a growing stagnant lid at the surface hampers heat loss from the mantle while its outer parts cools significantly, resulting in a thick magnetic layer when the core dynamo was active. If plate tectonics were active, for example as active as that examined by Breuer and Spohn [2003], then the crust was being formed at the ridge axes and being consumed at the trenches in a short time without appreciable cooling of its deeper parts. The residing time of a plate at the surface was short, and the magnetic layer was thin. Accordingly, plate tectonics can cool the interior of the planet efficiently, but retains only a thin magnetic layer at the surface. To investigate the potentially magnetic layer of Mars in case plate tectonics occurred during the active period of the core dynamo, we re-calculate the thermal evolution of the nominal model of Arkani-Hamed [2005] but modify it to allow the stagnant lid to grow after either 250 Myr or 500 Myr, implying that plate tectonics occurred within the first 250 or 500 Myr and Mars became a one-plate planet then after. The 500 Myr model is extreme, we do not promote such a long period for possible plate tectonic on early Mars. The calculations are made to simply show the extreme case scenario. Included in Figure 8 are the viscous demagnetization histories of these plate tectonic models since the cessation of the core dynamo. It is assumed that the upper parts of the plate with temperatures lower than the Curie temperature of a particular magnetic mineral were previously magnetized by the core field. The potentially magnetic layers of the plate tectonic models are thinner than that of the stagnant lithosphere. Likewise, the middle parts of the plates that are demagnetized through gradual viscous decay are thinner than that of the stagnant lid.

[25] Figure 9 shows the normalized magnetization of the magnetic layer at present for all of the stagnant lid thermal evolution models (Table 3), assuming that magnetite is the major magnetic carrier. The models are grouped to illustrate effects of major physical parameters on the viscous demagnetization of the magnetic layer. The models are identical to

the nominal model except for these major parameter values. Models 2, 4, 18, and 20 (Figure 9a) are identical to the nominal model, Model 9, except for the thickness of their initial crust, which contains 30% of the entire radioactive elements of the planet in all of these models. For example, the heat generation per unit volume of Model 2 with a 10 km thick initial crust is 5 times greater than that of Model 20 with 50 km thick initial crust. Despite strong enhancement of the heat generation per unit volume, the models with thinner crust have thicker magnetic layers because the heat produced in the crust readily escapes the planet. Models 7, 8, and 13 (Figure 9b) are identical to the nominal model except for the concentration of radioactive elements in their initial crust of 30 km thickness, which varies from 10% to 40% of the entire planet. The heat generation per unit volume in the crust of Model 7 is 4 times less than that of Model 13. The high rate of heat generation in the mantle of Model 7 enhances the mantle temperature and decreases the thickness of the potentially magnetic layer. The excess heat produced in the highly radioactive crust of Model 13 readily escapes the planet. The relatively less radioactive concentration in the mantle of this model results in reduced upper mantle temperature and a thicker magnetic layer.

[26] The most effective parameters are the initial temperature of the upper mantle and the total radioactive content of the planet. Models 5 and 17 (Figure 9c) are identical to the nominal model except for their initial upper mantle temperature. The lower the upper mantle temperature the thicker is the magnetic layer. The total radioactive contents of Models 14 and 15 (Figure 9d) are different from that of nominal model. Model 6 differs from the nominal model for its different Th/U and K/U ratios, which are terrestrial like. This model has the thickest potentially magnetic layer, whereas Model 14 with enhanced radioactive content has the thinnest layer. Changing the activation energy of the temperature-dependent viscosity from 300 KJ/mol of the nominal model to 540 KJ/mol of Model 22 has little effects on the magnetic layer (Figure 9e), whereas the reduced upper mantle viscosity of Model 23 enhances the heat flux to the stagnant lithosphere and results in a thinner magnetic layer. Other physical parameters such as the heat sources in the core, superheated initial core, and depth dependence of thermal expansion coefficient have minor effects on the thickness of the potentially magnetic layer and its viscous demagnetization.

[27] In general, hot models have thin magnetic layers at present, partly because they had already thin layers at the time the core dynamo ceased and partly because the thermal and viscous demagnetization were more effective since the cessation of the core dynamo. However, there are no distinct differences among the models as far as the viscous demagnetization of the lower parts of the magnetic layer is concerned despite appreciable variations of the physical parameters, except for Model 14 with large amount of radioactive elements. This model has the thinnest magnetic layer and thinnest viscous demagnetized zone.

4. Discussion and Conclusions

[28] An attempt is made in this paper to estimate effects of two factors on the possible demagnetization of Martian crust, the impact-induced shock pressure in the upper crust

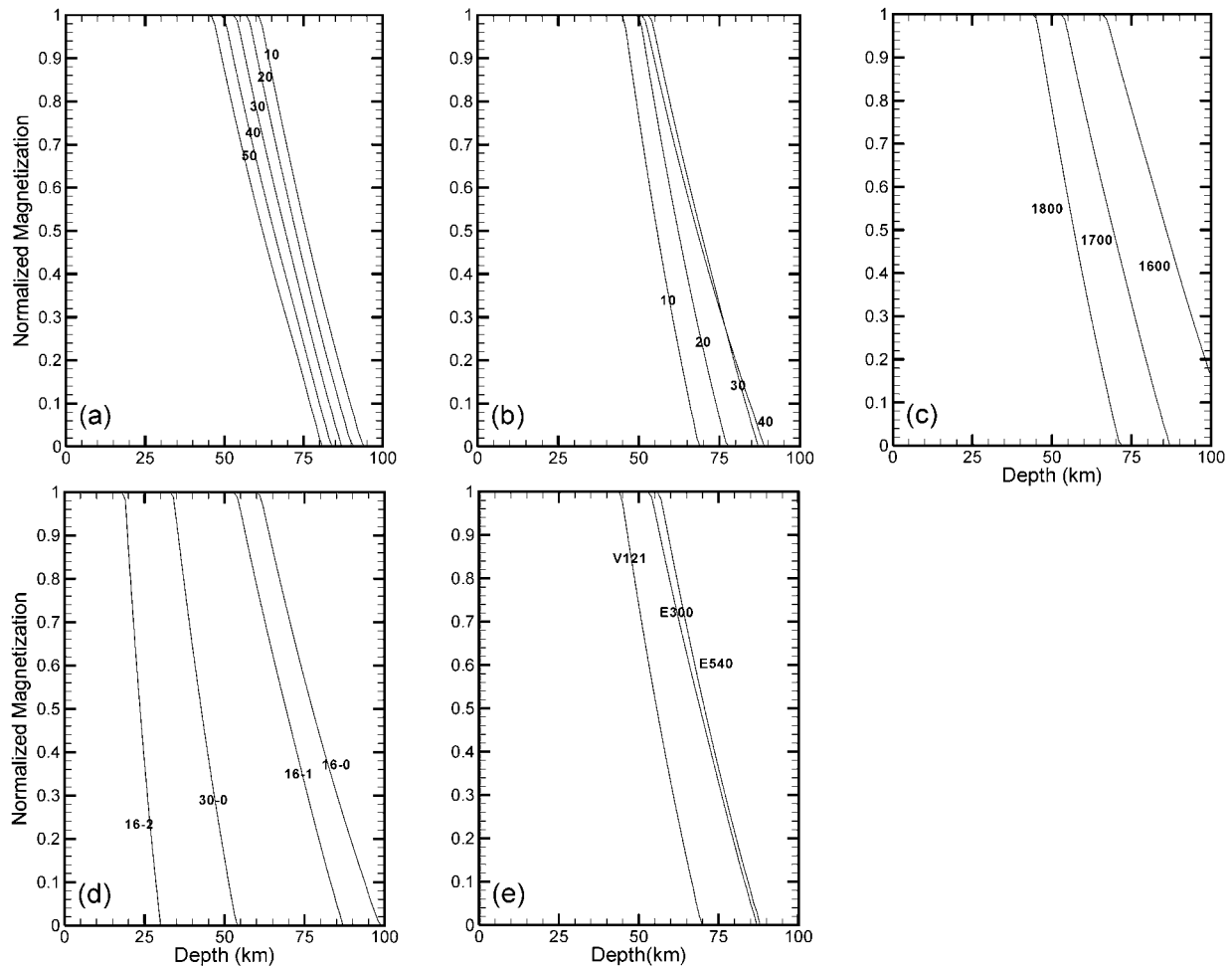


Figure 9. The present-day normalized magnetization of the magnetic layer. The numbers on the curves are as follows: (a) the thickness of the initial crust, in km; (b) the radioactive elements concentrated in the crust, in %; and (c) the initial temperature in the upper mantle at the bottom of the upper thermal boundary layer, in K. (d) The first number is the ppb average Uranium content of the planet at present, and the second number is 0 for terrestrial ratios of Th/U and K/U, 1 for the *Wänke and Dreibus* [1994] model, and 2 for the *Lodders and Fegley* [1997] model. (e) The curves E300 and E540 denote the activation energy in KJ/mol for the temperature-dependent viscosity, and the third curve shows Model 23 with reduced upper mantle viscosity.

and the gradual viscous decay in the deeper parts. Two scaling laws, H-S-H and Pi, are used to determine impact-induced shock pressure distribution in Martian lithosphere. It is shown that the former scaling law explains the demagnetized zones of the giant impacts basins Hellas, Isidis and Argyre better than the latter. We use 19 craters of diameters 300–600 km with well-defined topography to investigate the possible demagnetization of the crust by small to intermediate size impacts. We also adopt two magnetic intensity maps to detect the possible demagnetization of the crust. The majority of craters show no appreciable weakening of the magnetic intensity. Only three craters in the first map and two in the second map, show demagnetization in the inner area, but no appreciable weakening compared to the surrounding. Two craters of the first map and one crater of the second show magnetic weakening inside.

[29] Deeper part of the magnetic layer of Mars remains at high temperatures and likely loses part or all of its magnetization through viscous decay since the cessation of the core dynamo at ~ 4 Gyr ago. We investigate the gradual decay of magnetization on the basis of the thermal evolution models of Mars calculated using temperature and pressure dependent viscosity, temperature dependent thermal conductivity, depth dependent thermal expansion coefficient, time dependent radioactive heat generation, and different initial temperature distributions. A growing stagnant lithosphere is considered from the start in 23 models in order to investigate effects of different physical parameters on the resulting viscous demagnetization. Also, two additional viscous demagnetization models are calculated assuming that plate tectonics operated during the first 250 and 500 Myr and a stagnant lithosphere developed from then on. We investigate viscous magnetization assuming magnetite, hematite, or pyrrhotite as major magnetic carriers.

Majority of the stagnant lithosphere models show partial demagnetization within the lower ~ 30 km of the magnetic layer. The plate tectonic models have thinner magnetic layer than the stagnant lithosphere models.

[30] The demagnetization of the Martian crust depends on the coercivity of major magnetic minerals, magnetite, hematite, and pyrrhotite. *Robinson et al.* [2002] suggested lamellar magnetism of the hematite-ilmenite solid solution, which has a Curie temperature similar to that of magnetite, as a good candidate for producing planetary magnetic anomalies. The lamellar magnetism has the highest coercivity of the iron oxides, in the range 100–300 mT [*Kletetschka et al.*, 2002; *McEnroe et al.*, 2002]. *Cisowski and Fuller* [1978] found that remanent magnetization with a coercivity of 70 mT was $\sim 20\%$ demagnetized after a shock of 1 GPa and 70% after a shock of 4 GPa. Single domain magnetite and multidomain hematite also have high coercivity [*Kletetschka et al.*, 2000b]. Under a shock of 1 GPa, the remanent magnetization of the hematite-ilmenite lamella, single-domain magnetite, multidomain hematite and multidomain magnetite are reduced by 20%, 68%, 70%, and 85%, respectively [*Kletetschka and Wasilewski*, 2002]. The high pressure magnetic measurements in a diamond anvil cell show that magnetite behaves as single domain with high coercivity at high pressures [*Gilder et al.*, 2002]. The transient pressure produced by impact-induced shock waves is expected to have a similar result (the increase in coercivity would be somewhat less than that of an equivalent hydrostatic pressure; S. Gilder, personal communications, IGP, Paris, 2005). Low-coercivity titanomagnetite can be mostly demagnetized by shocks as low as 0.25 GPa [*Pohl et al.*, 1975]. At room temperatures, the coercivity of pyrrhotite samples analyzed by *Menyeh and O'Reilly* [1995] varied from 38 mT (for a grain size of 23–26 μm) to 63 mT (for a grain size of 2–5 μm), but dropped linearly to zero as temperature increased toward the Curie temperature. Shock experiments on high coercivity (300 mT) single domain pyrrhotite samples showed that a shock of 1 GPa removed 50% of the magnetization at room temperature, and they were completely demagnetized by shocks exceeding 2.75 GPa, undergoing a transition to a paramagnetic phase [*Rochette et al.*, 2003]. However, *Louzada et al.* [2005] suggested that pyrrhotite in meteorites shocked to pressures up to 4 GPa may still retain a pre-shock remanence likely hardened in coercivity and weakened in intensity by the shock. The survival of the magnetic anomalies beneath large craters can be partly due to the increase of coercivity during the passage of the shock wave.

[31] The impact-induced shock pressures based on the H-S-H scaling, which are larger than those predicted by the Pi scaling, suggest that impacts creating craters larger than 300 km in diameter are capable of producing shock pressures in excess of 2 GPa in the entire magnetic layer beneath $\sim 80\%$ of the crater's radius. The rock magnetic measurements suggest that a magnetized rock loses part of its magnetization when subjected to shock pressures of a few GPa [e.g., *Cisowski and Fuller*, 1978; *Kletetschka and Wasilewski*, 2002; *Kletetschka et al.*, 2004]. It is therefore expected to detect the demagnetization of the Martian crust by large impacts. As a matter of fact all giant basins, Hellas, Isidis, and Argyre do show almost complete demagnetization of the magnetic layer beneath the major parts of the

basins. *Mohit and Arkani-Hamed* [2004] identified a few large craters where magnetic anomalies are somewhat reduced. We investigated 19 craters with diameters of 300–600 km and distinct topographic signatures using two magnetic anomaly maps. Nine of the craters were among the 12 craters studied by *Mohit and Arkani-Hamed* [2004] who concluded that the impacts had minor effects on the magnetization of the crust. Our results also show no robust correlation between the impact sites and expected demagnetization of the magnetic layer. It is worth mentioning that there is no direct relationship between the magnetization and the magnetic field of a given body. For example, the maximum intensity of the magnetic field produced by a uniformly magnetized circular disk occurs directly above the center of the disk only when the magnetization is vertical, but it is displaced relative to the center when the magnetization has appreciable inclination. The displacement depends on the size of the disk, the altitude of the magnetic field observation, and the inclination of the magnetization vector. The maximum magnetic intensity usually occurs above the disk when the disk diameter is comparable to the observation altitude. Therefore the impact demagnetization may not result in weakening of the magnetic intensity directly over the entire crater.

[32] It is possible that the potentially magnetic layer is much thicker than the one we have considered. Either the mantle of Mars is magnetic and its uppermost parts were magnetized by the core field, or the crust is much thicker. The Earth's mantle beneath continents seems to be non-magnetic [*Wasilewski et al.*, 1979], though we cannot use this to argue strictly for a non-magnetic Martian mantle because there is no direct information about the actual oxidation state of iron in the Martian mantle. There are, however, ample amounts of evidence that Mars has become a one-plate planet in the early history [see *Solomon et al.*, 2005, and references therein]. A growing stagnant lid would have hampered heat loss from the interior and kept the upper mantle at a high temperature during the active period of the core dynamo, because of the significant amounts of heat generated by the high concentration of radioactive elements in the early history of the planet.

[33] It is possible that many of the craters we considered have been produced before the magnetic source bodies acquired their magnetization. This is certainly a possibility if the source bodies are intrusive [e.g., *Kletetschka et al.*, 2005]. The cratering history of Mars is not well understood, whether cratering was a more or less continuous process until it sharply reduced at about 4 Gyr ago or there was catastrophic cratering in the vicinity of 4 Ga [e.g., *Hartmann and Neukum*, 2001]. If the core dynamo ceased much later than the final period of intensive cratering, it is possible for intrusive bodies that penetrated the crust after the intensive cratering but before the cessation of the core dynamo to cool appreciably and acquire magnetization.

[34] It is also possible that the scaling laws established for small craters in the calculations of the shock pressure distribution are not applicable to large impacts occurred during the early history of Mars. The two scaling laws we examined result in substantially different impact pressure distributions. However, in the absence of other information extrapolating the scaling laws to large craters seems to be a viable option.

[35] Finally, there are possibly other processes that have effected the magnetization of the Martian lithosphere. For example, faults and cracks created in crust may have allowed surface water, probably existed on the ancient Mars, penetrate the crust and decrease its magnetization through low-temperature hydration [e.g., *Solomon et al.*, 2005]. The low-temperature hydration is mainly responsible for the reduction of the magnetization of the oceanic crust on Earth by a factor of about 5 within less than 20 Myr [e.g., *Bleil and Petersen*, 1983]. Also, emplacement of thick basaltic lava at the surface could have thermally demagnetized the near surface parts [e.g., *Arkani-Hamed*, 2004; *Johnson and Phillips*, 2004]. The present paper is concerned with two of the processes, the impact-induced shock pressure and the viscous magnetization. It is quite possible that different processes have operated during the long history of the planet's history. Attempts have been made by many authors to understand the nature of the magnetic sources of Mars that give rise to the strong magnetic anomalies of Cimmeria and Sirenum Terrae. The nature of the sources will remain poorly understood until we obtain very low altitude magnetic data and conduct rock magnetic analysis of the Martian rocks.

[36] **Acknowledgments.** This research is supported by Natural Sciences and Engineering Research Council (NSERC) of Canada to J. Arkani-Hamed. We would like to thank Herbert Frey at Goddard Space Flight Center for providing his crater catalog and David Mitchell at Berkeley for providing the magnetic map of Mars at 170 km altitude derived from the Electron Reflectometer data. Discussions with David Dunlop at University of Toronto and Stuart Gilder at IPGP, Paris, were very helpful. We would also like to thank the Associate Editor Francis Nimmo and the two anonymous reviewers for their constructive comments.

References

- Acuna, M. H., et al. (1999), Global distribution of crustal magnetization discovered by the Mars Global Surveyor MAG/ER experiment, *Science*, *284*, 790–793.
- Arkani-Hamed, J. (2003), Thermoremanent magnetization of the Martian lithosphere, *J. Geophys. Res.*, *108*(E10), 5114, doi:10.1029/2003JE002049.
- Arkani-Hamed, J. (2004), Timing of the Martian core dynamo, *J. Geophys. Res.*, *109*, E03006, doi:10.1029/2003JE002195.
- Arkani-Hamed, J. (2005), Magnetic crust of Mars, *J. Geophys. Res.*, *110*, E08005, doi:10.1029/2004JE002397.
- Bleil, U., and N. Petersen (1983), Variations in magnetization intensity and low-temperature titanomagnetite oxidation of ocean floor basalts, *Nature*, *301*, 384–388.
- Breuer, D., and T. Spohn (2003), Early plate tectonics versus single-plate tectonics on Mars: Evidence from magnetic field history and crust evolution, *J. Geophys. Res.*, *108*(E7), 5072, doi:10.1029/2002JE001999.
- Breuer, D., and T. Spohn (2006), Viscosity of the Martian mantle and its initial temperature: Constraints from crust formation history and the evolution of the magnetic field, *Planet. Space Sci.*, *54*, 153–169.
- Cain, J. C., B. B. Ferguson, and D. Mozzoni (2003), An $n = 90$ internal potential function of the Martian crustal magnetic field, *J. Geophys. Res.*, *108*(E2), 5008, doi:10.1029/2000JE001487.
- Cisowski, S. M., and M. Fuller (1978), The effect of shock on the magnetism of terrestrial rocks, *J. Geophys. Res.*, *83*, 3441–3458.
- Cisowski, S. M., and M. Fuller (1982), The role of impact magnetization in the solar system, *Adv. Space Res.*, *2*, 35–39.
- Connerney, J. E. P., M. H. Acuna, P. Wasilewski, N. F. Ness, H. Rème, C. Mazelle, D. Vignes, R. P. Lin, D. Mitchell, and P. Cloutier (1999), Magnetic lineations in the ancient crust of Mars, *Science*, *284*, 794–798.
- Dunlop, D. J., and J. Arkani-Hamed (2005), Magnetic minerals in the Martian crust, *J. Geophys. Res.*, *110*, E12S04, doi:10.1029/2005JE002404.
- Dunlop, D. J., and G. Kletetschka (2001), Multidomain hematite: A source of planetary magnetic anomalies?, *Geophys. Res. Lett.*, *28*, 3345–3348.
- Dunlop, D. J., and Ö. Özdemir (1997), *Rock Magnetism: Fundamentals and Frontiers*, 573 pp., Cambridge Univ. Press, New York.
- Dunlop, D. J., Ö. Özdemir, D. A. Clark, and P. W. Schmidt (2000), Time-temperature relations for the remagnetization of pyrrhotite (Fe_7S_8) and their use in estimating paleotemperatures, *Earth Planet. Sci. Lett.*, *176*, 107–116.
- Ebbing, J., P. Janle, J. Koulouris, and B. Milkereit (2001), 3D gravity modeling of the Chicxulub impact structure, *Planet. Space Sci.*, *49*, 599–609.
- Frey, H. V. (2003), Large-diameter visible and buried impact basins on Mars: Implications for the age of the highlands and (buried) lowlands and turn-off of the global magnetic field, *Lunar Planet. Sci.*, XXXIV, Abstract 1838.
- Frey, H. V., G. J. Hohner, A. Wernecke, J. H. Roark, and S. E. Sakimoto (2002), Buried impact basins as constraints on the thickness of ridged plains and northern lowland on Mars, *Lunar Planet. Sci.*, XXXIII, Abstract 1894.
- Gault, D. E. (1974), Impact cratering, in *A Primer of Lunar Geology*, edited by R. Greeley and P. Schultz, pp. 137–175, NASA Ames Res. Cent., Moffett Field, Calif.
- Gilder, S. A., M. LeGoff, J. Peyronneau, and J. Chervin (2002), Novel high pressure magnetic measurements with application to magnetite, *Geophys. Res. Lett.*, *29*(10), 1392, doi:10.1029/2001GL014227.
- Gilder, S. A., M. LeGoff, J.-C. Chervin, and J. Peyronneau (2004), Magnetic properties of single and multi-domain magnetite under pressures from 0 to 6 GPa, *Geophys. Res. Lett.*, *31*, L10612, doi:10.1029/2004GL019844.
- Halekas, J. S., D. L. Mitchell, R. P. Lin, L. L. Hood, M. H. Acuña, and A. B. Binder (2002), Demagnetization signatures of lunar impact craters, *Geophys. Res. Lett.*, *29*(13), 1645, doi:10.1029/2001GL013924.
- Hargraves, R. B., J. M. Knudsen, M. B. Madsen, and P. Bertelsen (2001), Finding the right rocks on Mars, *Eos Trans. AGU*, *82*, 292–293.
- Hartmann, W., and G. Neukum (2001), Cratering chronology and the evolution of Mars, *Space Sci. Rev.*, *96*, 165–194.
- Hauck, S. A., II, and R. J. Phillips (2002), Thermal and crustal evolution of Mars, *J. Geophys. Res.*, *107*(E7), 5052, doi:10.1029/2001JE001801.
- Holsapple, K. A. (1993), The scaling of impact processes in planetary sciences, *Annu. Rev. Earth Planet. Sci.*, *21*, 333–373.
- Hood, L. L., N. C. Richmond, E. Pierazzo, and P. Rochette (2003), Distribution of crustal magnetic fields on Mars: Shock effects of basin-forming impacts, *Geophys. Res. Lett.*, *30*(6), 1281, doi:10.1029/2002GL016657.
- Johnson, C. L., and R. J. Phillips (2004), Evolution of the Tharsis region of Mars: Insights from magnetic field observations, *Earth Planet. Sci. Lett.*, *230*, 241–254.
- Kletetschka, G., and P. J. Wasilewski (2002), Grain size limit for SD hematite, *Phys. Earth Planet. Inter.*, *129*, 173–179.
- Kletetschka, G., P. J. Wasilewski, and P. T. Taylor (2000a), Mineralogy of the sources for magnetic anomalies on Mars, *Meteorit. Planet. Sci.*, *35*, 895–899.
- Kletetschka, G., P. J. Wasilewski, and P. T. Taylor (2000b), Unique thermoremanent magnetization of multidomain sized hematite: Implications for magnetic anomalies, *Earth Planet. Sci. Lett.*, *176*, 469–479.
- Kletetschka, G., P. J. Wasilewski, and P. T. Taylor (2002), The role of hematite-ilmenite solid solution in the production of magnetic anomalies in ground- and satellite-based data, *Tectonophysics*, *347*, 167–177.
- Kletetschka, G., J. E. P. Connerney, N. F. Ness, and M. H. Acuna (2004), Pressure effects on Martian crustal magnetization near large impact basins, *Meteorit. Planet. Sci.*, *39*, 1839–1848.
- Kletetschka, G., N. F. Ness, J. E. P. Connerney, N. F. Ness, M. H. Acuna, and P. J. Wasilewski (2005), Grain size dependent potential for self generation of magnetic anomalies on Mars via thermoremanent magnetic acquisition and magnetic interaction of hematite and magnetite, *Phys. Earth Planet. Inter.*, *148*, 149–156.
- Langlais, B., M. E. Purucker, and M. Manda (2004), Crustal magnetic field of Mars, *J. Geophys. Res.*, *109*, E02008, doi:10.1029/2003JE002048.
- Lodders, K., and B. Fegley (1997), An oxygen isotope model for the composition of Mars, *Icarus*, *126*, 373–394.
- Louzada, K. L., S. T. Stewart, and B. P. Weiss (2005), Shock demagnetization of pyrrhotite, *Lunar Planet. Sci.*, XXXVI, Abstract 1134.
- McEnroe, S. A., R. J. Harrison, P. Robinson, and F. Langenhorst (2002), Nanoscale haematite-ilmenite lamellae in massive ilmenite rock: An example of 'lamellar magnetism' with implications for planetary magnetic anomalies, *Geophys. J. Int.*, *151*, 890–912.
- Melosh, H. J. (1989), *Impact Cratering: A Geologic Process*, Oxford Univ. Press, New York.
- Menyeh, A., and W. O'Reilly (1995), The coercive force of fine particles of monoclinic pyrrhotite (Fe_7S_8) studied at elevated temperature, *Phys. Earth Planet. Inter.*, *89*, 51–62.
- Mitani, N. K. (2003), Numerical simulations of shock attenuation in solids and reevaluation of scaling law, *J. Geophys. Res.*, *108*(E1), 5003, doi:10.1029/2000JE001472.

- Mitchell, D. L., R. P. Lin, C. Mazelle, H. Rème, P. A. Cloutier, J. E. P. Connerney, M. H. Acuña, and N. F. Ness (2001), Probing Mars' crustal magnetic field and ionosphere with the MGS Electron Reflectometer, *J. Geophys. Res.*, *106*(E10), 23,419–23,428.
- Mohit, P. S., and J. Arkani-Hamed (2004), Impact demagnetization of the Martian crust, *Icarus*, *168*, 305–317.
- Neukum, G., and D. V. Wise (1976), Mars: A standard crater curve and possible new time scale, *Science*, *194*, 1381–1387.
- Neumann, G. A., M. T. Zuber, M. A. Wieczorek, P. J. McGovern, F. G. Lemoine, and D. E. Smith (2004), Crustal structure of Mars from gravity and topography, *J. Geophys. Res.*, *109*, E08002, doi:10.1029/2004JE002262.
- Nimmo, F., and M. S. Gilmore (2001), Constraints on the depth of magnetized crust on Mars from impact craters, *J. Geophys. Res.*, *106*(E6), 12,315–12,323.
- Nimmo, F., and D. J. Stevenson (2000), Influence of early plate tectonics on the thermal evolution and magnetic field of Mars, *J. Geophys. Res.*, *105*, 11,969–11,979.
- Norman, M. D. (1999), The composition and thickness of the crust of Mars estimated from rare earth elements and neodymium-isotopic compositions of Martian meteorites, *Meteorit. Planet. Sci.*, *34*, 439–449.
- Norman, M. D. (2002), Thickness and composition of the Martian crust revisited: Implications of an ultradepleted mantle with a Nd isotope composition like that of QUE94201, *Proc. Lunar Planet. Sci. Conf. 33rd*, Abstract 1175.
- Pierazzo, E., A. M. Vickery, and H. J. Melosh (1997), A reevaluation of impact melt production, *Icarus*, *127*, 408–423.
- Pilkington, M., and A. R. Hildebrand (2000), Three-dimensional magnetic imaging of the Chicxulub crater, *J. Geophys. Res.*, *105*, 23,479–23,491.
- Pohl, J., U. Bleil, and U. Hornemann (1975), Shock magnetization and demagnetization of basalt by transient stress up to 10 kbar, *J. Geophys.*, *41*, 23–41.
- Pullaiah, G., E. Irving, K. L. Buchan, and D. J. Dunlop (1975), Magnetization changes caused by burial and uplift, *Earth Planet. Sci. Lett.*, *28*, 133–143.
- Robinson, P., R. J. Harrison, S. A. McEnroe, and R. B. Hargraves (2002), Lamellar magnetism in the hematite-ilmenite series as an explanation for strong remanent magnetization, *Nature*, *418*, 517–520.
- Rochette, P., J.-P. Lorand, G. Fillion, and V. Sautter (2001), Pyrrhotite and the remanent magnetization of SNC meteorites: A changing perspective on Martian magnetism, *Earth Planet. Sci. Lett.*, *190*, 1–12.
- Rochette, P., G. Fillion, R. Ballou, F. Brunet, B. Ouladdiaf, and L. Hood (2003), High pressure magnetic transition in pyrrhotite and impact demagnetization on Mars, *Geophys. Res. Lett.*, *30*(13), 1683, doi:10.1029/2003GL017359.
- Schmidt, R. M., and K. R. Housen (1987), Some recent advances in the scaling of impact and explosion cratering, *Int. J. Impact Eng.*, *5*, 543–560.
- Schult, A. (1970), Effect of pressure on the Curie temperature of titanomagnetites $(1 - x)Fe_3O_4 - xTiFe_2O_4$, *Earth Planet. Sci. Lett.*, *10*, 81–86.
- Scott, R. G., M. Pilkington, and E. I. Tanczyk (1997), Magnetic investigations of the West Hawk, Deep Bay and Clearwater impact structures, Canada, *Meteorit. Planet. Sci.*, *32*, 293–308.
- Sleep, N. H. (1994), Martian plate tectonics, *J. Geophys. Res.*, *99*, 5639–5665.
- Solomon, S. C., et al. (2005), New perspectives on ancient Mars, *Science*, *307*, 1214–1220.
- Turcotte, D. L., and G. Schubert (1982), *Geodynamics*, 450 pp., John Wiley, Hoboken, N. J.
- Turcotte, D. L., R. Shcherbakov, B. D. Malamud, and A. B. Kucinskas (2002), Is the Martian crust also the Martian elastic lithosphere?, *J. Geophys. Res.*, *107*(E11), 5091, doi:10.1029/2001JE001594.
- Wänke, H., and G. Dreibus (1994), Chemistry and accretion of Mars, *Philos. Trans. R. Soc. London, Ser. A*, *349*, 2134–2137.
- Wasilewski, P. J., H. H. Thomas, and M. A. Mayhew (1979), The Moho as a magnetic boundary, *Geophys. Res. Lett.*, *6*, 541–544.
- Werner, S. C., J. Plado, L. J. Pesonen, P. Janle, and S. Elo (2002), Potential fields and subsurface models of Suvasvesi North impact structure, Finland, *Phys. Chem. Earth*, *27*, 1237–1245.
- Whaler, K. A., and M. E. Purucker (2005), A spatially continuous magnetization model for Mars, *J. Geophys. Res.*, *110*, E09001, doi:10.1029/2004JE002393.

J. Arkani-Hamed and H. Shahnas, Department of Physics, University of Toronto, 60 St. George Street, Toronto, ON, Canada M5S 1A7. (jafar@physics.utoronto.ca; shahnas@physics.utoronto.ca)